Disrupting inter-subunit interactions favors channel opening in P2X2 receptors

Federica Gasparri, Sarune Bielickaite, Mette Homann Poulsen, Stephan Alexander Pless*

Center for Biopharmaceuticals, Department of Drug Design and Pharmacology, University of Copenhagen, 2100 Copenhagen, Denmark

* Corresponding author:

Stephan Pless

Center for Biopharmaceuticals

Department of Drug Design and Pharmacology

University of Copenhagen

Jagtvej 160, 2100 Copenhagen, Denmark

Mail: stephan.pless@sund.ku.dk

ABSTRACT

P2X receptors (P2XRs) are trimeric ligand-gated ion channels that open a cation-selective pore in response to ATP binding to their large extracellular domain (ECD). The seven known P2XR subtypes typically assemble as homo- or heterotrimeric complexes and they contribute to numerous physiological functions, including nociception, inflammation and hearing. Both the overall structure of P2XRs and the details of how ATP is coordinated at the subunit interface are well established. By contrast, little is known about how inter-subunit interactions in the ECD contribute to channel function. Here we investigate both single and double mutants at the subunit interface of rP2X2Rs using electrophysiological and biochemical approaches. Our data demonstrate that the vast majority of mutations that disrupt putative inter-subunit interactions result in channels with higher apparent ATP affinity and that double mutants at the subunit interface show significant energetic coupling, especially if the mutations are located in close proximity. Overall, we show that inter-subunit interactions, as well as possibly interactions in other parts of the receptor, stabilize WT rP2X2Rs in the closed state. This suggests that, unlike other ligand-gated ion channels, P2X2 receptors have not evolved for an intrinsically low threshold for activation, possibly to allow for additional modulation or as a cellular protection mechanism against overstimulation.

INTRODUCTION

Release of ATP into the extracellular milieu can activate a class of trimeric ligand-gated ion channels known as P2X receptors (P2XRs) (G. Burnstock, 1972; Coddou et al., 2011). Upon ATP binding, these membrane-spanning proteins open a cation-selective pore and contribute to a variety of physiological processes. These include nociception, sensory transduction, inflammatory processes and muscle contraction, highlighting P2XRs as potential drug targets (Arulkumaran et al., 2011; Broom et al., 2008; Geoffrey Burnstock, 2007; Finger et al., 2005; Illes et al., 2020; Jarvis et al., 2002; Khakh & North, 2012). Seven P2XR isoforms (P2X1-7) are known in humans, and they display tissue-specific expression patterns and most subunits can assemble as homo- or heterotrimeric receptors. For example, homomeric P2X2Rs are involved in hearing (George et al., 2019; Zhu et al., 2017) and P2X2/P2X3 heteromeric receptors are implicated in nociceptive pathways (Carter et al., 2009; Honore et al., 2006; Stephan et al., 2018).

A number of recent structural studies have provided unprecedented insight into the three-dimensional architecture of P2XRs (Hattori & Gouaux, 2012; Karasawa & Kawate, 2016; Kasuya et al., 2016; Kasuya, Fujiwara, et al., 2017; Kasuya, Yamaura, et al., 2017; Kawate et al., 2009; Mansoor et al., 2016; McCarthy et al., 2019; Wang et al., 2018). Overall, the receptors adopt a chalice-shaped trimeric structure with each subunit roughly resembling the outline of a dolphin: the two helices (M1 and M2) of the transmembrane domain (TMD) form the fluke, while the large extracellular domain makes up the body with attached dorsal fin, flippers and head domains (Kawate et al., 2009) (Figure 1). The ATP binding site is located at the interface of two adjacent subunits and the contributions by conserved side chains or backbone atoms to the coordination of the ligand molecule have been investigated thoroughly (Chataigneau et al., 2013; Ennion et al., 2000; Gasparri et al., 2019; L. H. Jiang et al., 2000; Kasuya, Fujiwara, et al., 2017; Roberts et al., 2008; Roberts & Evans, 2006). The binding of ATP is thought to cause a series of conformational steps that ultimately trigger channel opening. Initially, a tightening of the jaw region around the ATP binding site causes a displacement of the surrounding flexible regions, dorsal fin and flippers. These movements exert tension on the β-sheet wall across upper and lower body, causing it to flex outward, enlarge the lateral fenestration present in the lower body region and, in turn, open the transmembrane pore (Chataigneau et

al., 2013; Mansoor et al., 2016). This view is supported by several functional studies using disulfide bridging, affinity labeling, voltage-clamp fluorometry studies and molecular dynamic simulations (Hausmann et al., 2013; Huang et al., 2014; R. Jiang et al., 2011, 2012; Lörinczi et al., 2012; Roberts et al., 2012; Stelmashenko et al., 2014; Zhao et al., 2014). However, it remains unclear to what degree the extensive interactions across the subunit interfaces affect this process, i.e. if disruptions of these interactions would favor channel opening or closing.

In this study, we focused primarily on interactions formed at the extracellular subunit interfaces in rP2X2Rs and we hypothesized that mutational disruptions would impact channel function. Indeed, we show that interfering with putative inter-subunit interactions favors channel opening, as close to 90% of the examined mutants (20/23) displayed a significantly *reduced* EC_{50} for ATP. We further use double-mutant cycle analysis to demonstrate that the majority of tested sites show strong energetic coupling, thus revealing a tight interplay between residues throughout the ECD. Together, our data demonstrate that inter-subunit interactions are crucial for fine-tuning ATP sensitivity and, unusually, contribute towards lowering the apparent agonist affinity of rP2X2Rs.

RESULTS

Single point mutations at the inter-subunit interface increase ligand sensitivity

The apo and ATP-bound zebrafish P2X4R structures (PDB 315D and 4DW1(Hattori & Gouaux, 2012; Kawate et al., 2009)) were analyzed using the PISA (Protein, Interfaces, Structures and Assemblies (EMBL-EBI, n.d.)) program to pinpoint residues at the interface between P2XR subunits that form H-bonds and/or salt bridges in both conformational states (Figure 1, Supplementary Table 1). Specifically, we focused on the extracellular domain, in analogy to a previous study (Hausmann et al., 2014). To asses if these interactions are conserved in P2X2Rs, we used a sequence alignment to identify the corresponding residues in the rP2X2R subtype. We excluded side chains at the ATP binding pocket, which have been extensively characterized previously (Chataigneau et al., 2013; Gasparri et al., 2019; L. H. Jiang et al., 2000), and instead focused on mutating residues that would disrupt putative inter-subunit interactions distant from the ligand binding pocket, as highlighted in the rP2X2 homology model shown in Figure 1.

A

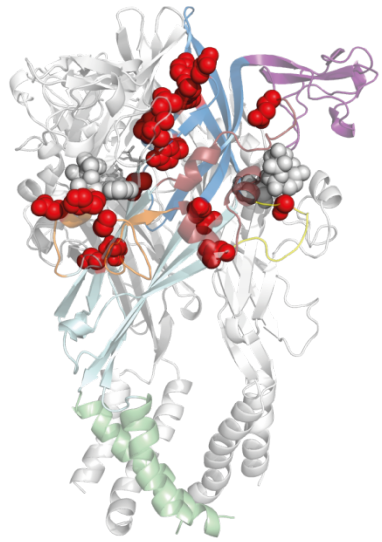

B

Predicted inter-subunit interactions

Subunit A	Subunit B
S65	R313
I66	R313
I73	L135
D78	L112
K79	T302
V80	L110
E84	Y294
Y86	T302
E91	G92
S190	L278
G201	L276
G201	S284
D209	P282
H213	Q138
C214[1]	Q138
K293	T302
Y295	T302

Figure 1: Overview of P2XR structure and residues at subunit interface. *(A) Homology model of rP2X2R based on the X-ray crystal structure of the ATP-bound zebrafish P2X4R. One of the three subunits is color-coded: the two TM helices forming the fluke in green; lower and upper body in light and dark blue, respectively; the head domain in purple; the dorsal fin in orange and the flippers in yellow and red. The ATP molecules are shown in light grey spheres. The side chains at the subunit interface mutated in this study are highlighted with red spheres. (B) Table of side chains predicted to interact across the inter-subunit interface. The side chains mutated to disrupt a given interaction are*

shown in black font, the others in grey font. [1]: Residue involved in disulfide bond, therefore not considered here. Note that due to sequence differences between P2X2 and P2X4 not all residues/interactions are conserved.

Single rP2X2R mutants were expressed in *Xenopus laevis* oocytes and currents in response to ATP application were measured using two-electrode voltage-clamp (TEVC). Analysis of concentration-response curves (CRCs) showed that 14 of the 17 single mutants responded to lower concentrations of ATP than WT rP2X2R, resulting in significantly reduced EC_{50} values (Figure 2, Table 1). Six of these 14 mutants (S65A, E84Q, S190A, L276A, K293Q, Y295F) showed ~ 10-fold decrease in EC_{50}, while K79Q did not change the EC_{50} compared to WT and I73A and V80A both resulted in nearly two- and three-fold increase in EC_{50} (Table 1).

Next, we wanted to assess if inter-subunit residues in the transmembrane domain (TMD) would also affect the ATP EC_{50} value, as for example suggested by the constitutively active phenotype of a P2X2R M1 mutation involved in hearing loss (V60L)(George et al., 2019). The hydroxyl moiety of the tyrosine in position 43 points towards the M2 helix of the adjacent subunit and single point mutations to either alanine or phenylalanine resulted in a pronounced left-shift in the ATP CRCs compared to the WT (Table 1). This indicates that disruptions to inter-subunit interactions in both the TMD and in the ECD, not involved in ATP binding, are crucial for channel gating. Interestingly, mutating single residues most often resulted in phenotypes with increased ATP apparent affinity.

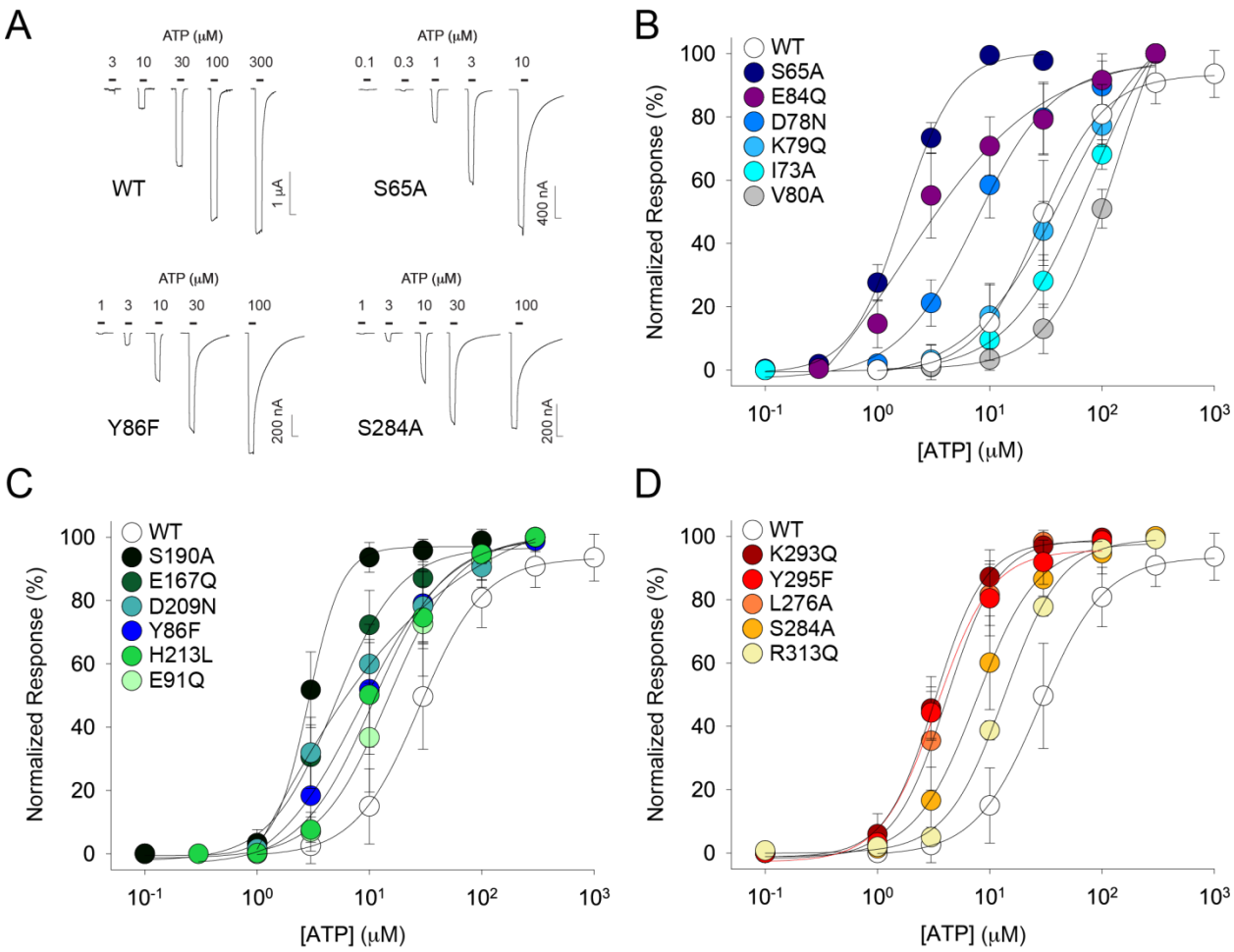

Figure 2: Characterization of single point mutations at the inter-subunit interfaces of rP2X2R. *(A) Example recordings of rP2X2 WT, S65A, Y86F and S284A receptors. Currents are elicited by increasing concentration of ATP (black bars). Scale bar: x, 10 s y, nA/μA. (B)-(D) Normalized ATP-elicited concentration-response data for WT and indicated mutant rP2X2Rs in response to increasing concentrations of ATP. Data are displayed as mean ± S.D. (n = 6-24).*

Most double mutants at the same subunit interface show energetic coupling

Next, we sought to investigate if introduction of double mutants at the inter-subunit interface would result in additive effect in rP2X2R ATP apparent affinity. In a trimeric channel, there are three equivalent subunit interfaces within each fully assembled receptor. Here, we first generated a series of double mutants in which each of the inter-subunit interfaces was disrupted by two of the above characterized single mutations

situated on an interface facing the *same* subunit. Specifically, we generated the S284A/L276A, Y86F/K293Q, E84Q/E91Q, D78N/S190A and V80A/S190A mutations (Figure 3A).

Both L276 and S284 are situated on the left flipper region and, when mutated to alanine, reduced the EC_{50} values to < 10 μM (Figure 3B and Table 1). If the two mutations were energetically uncoupled, we would expect the effects on the EC_{50} to be additive, i.e. the S284A/L276A double mutant to display an even more reduced EC_{50} value. However, we determined the S284A/L276A double mutant EC_{50} to be indistinguishable from that of the S284A single mutant (Figure 3B). We calculated the coupling energy between the two mutants to be 4.9 kJ mol^{-1}, indicating strong energetic coupling (Table 2). Despite being located distant from the S284A/L276A pair, the Y86F/K293Q double mutant in the upper body resulted in an almost identical coupling energy (5.3 kJ mol^{-1}; Figure 3C Table 2). Strikingly, the E84Q/E91Q double mutant pair (both positions are located between the β3-β4 sheets) displayed a 20-fold increase in EC_{50} compared to that of the WT, and in stark contrast to the reduced EC_{50}s observed with the two single mutants (Figure 3D, Table 1 and 2). Indeed, double-mutant cycle analysis revealed a very strong coupling of the E84/E91 pair (14.7 kJ mol^{-1}).

Next, we sought to interrogate potential upper-lower body interactions through different combinations of mutants at S190 (β8-sheet), D78 (β3-sheet) and V80 (β3-sheet). The D78N/S190A double mutant showed a lower EC_{50} compared to each of the underlying single mutants (Figure 3E, Table 2). Consequently, the change in free energy of approximately 1.3 kJ mol^{-1} indicated a small degree of coupling. Similarly, the V80A/S190A double mutant showed virtually no change in free energy (0.7 kJ mol^{-1}; Figure 3F, Table 2), as the ATP apparent affinity is roughly intermediate between the two single mutants.

Together, this suggests that double mutants within the flipper domain, as well as within the upper body show strong energetic coupling, while no such coupling could be observed between more distant upper-lower body pairs.

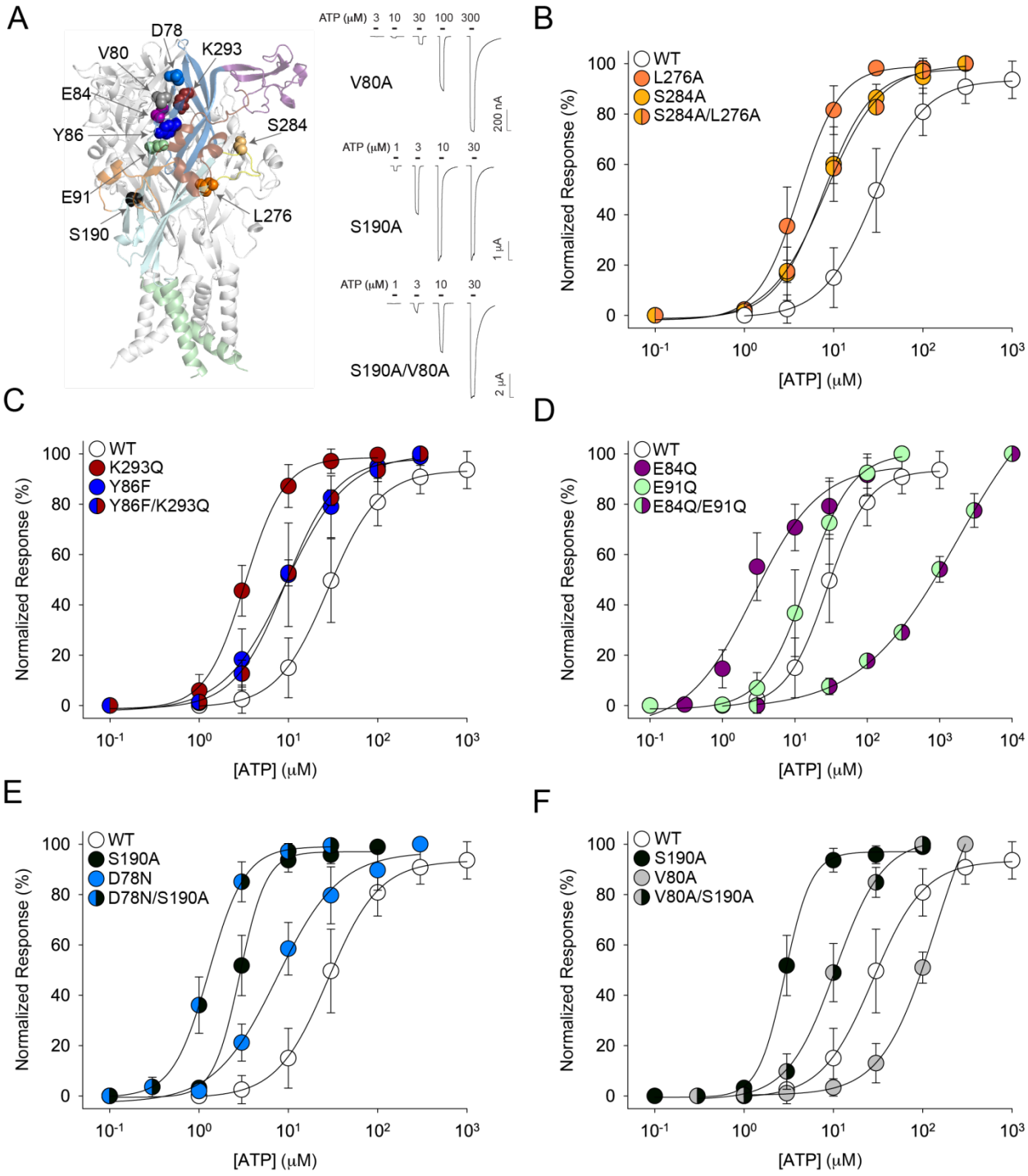

Figure 3: Characterization of double mutants disrupting the same subunit interface. *(A, left) Homology model of rP2X2R with residues corresponding to the positions mutated shown as spheres (same colour scheme as Figure 2). (A, right) Example recordings of V80A, S190A and V80A/S190A mutants. Currents are elicited by increasing concentration of ATP (black bars). Scale bar: x, 10 s y, nA/μA. (B to F) Normalized ATP-elicited concentration-response data for WT (empty symbols), single (single-colour symbols) and double mutants (split-colour symbols) rP2X2Rs in response to increasing concentrations of ATP. Data are shown as mean ± S.D. (n = 4-24).*

Double mutants at different subunit interfaces show energetic coupling or prevent expression

Next, we generated a set of double mutants in which each of the inter-subunit interfaces was disrupted by two of the above characterized single mutations situated on an interface facing a *different* subunit. Specifically, three positions in the upper body D78, Y86 and E91 (in β3-β4 sheet and loop) were mutated in combination with side chains from the head domain (E167), left flipper (L276) or lower body (R313) to investigate if double mutations would be energetically coupled (Figure 4A).

The E91Q/R313Q and D78N/E167A double mutants did not show any ATP-gated inward currents, even in response to high (10 mM) concentrations of ATP. In order to assess if this was due to severe gating phenotypes or rather surface expression, we performed a surface biotinylation assay, followed by Western blotting. As shown in Figure 4B, bands corresponding to a rP2X2R-sized protein are absent for the E91Q/R313Q and the D78N/E167A double mutant channels in both the surface fraction and the total lysate, suggesting that these double mutants are not expressed in *Xenopus laevis* oocytes (Figure 4B and Supplementary Figure 1).

By contrast, the Y86F/L276A and D78N/L276A double mutants displayed an EC_{50} similar to that observed with the single mutants, i.e. significantly left-shifted compared to WT rP2X2R (Figure 4C/D, Table 2). We performed double-mutant cycle analysis to assess a potential energetic coupling between these mutations. This yielded coupling energies of 5.1 kJ mol^{-1} for Y86F/L276A and of 2.8 kJ mol^{-1} for D78N/L276A (Table 2), suggesting strong energetic coupling between these side chain pairs.

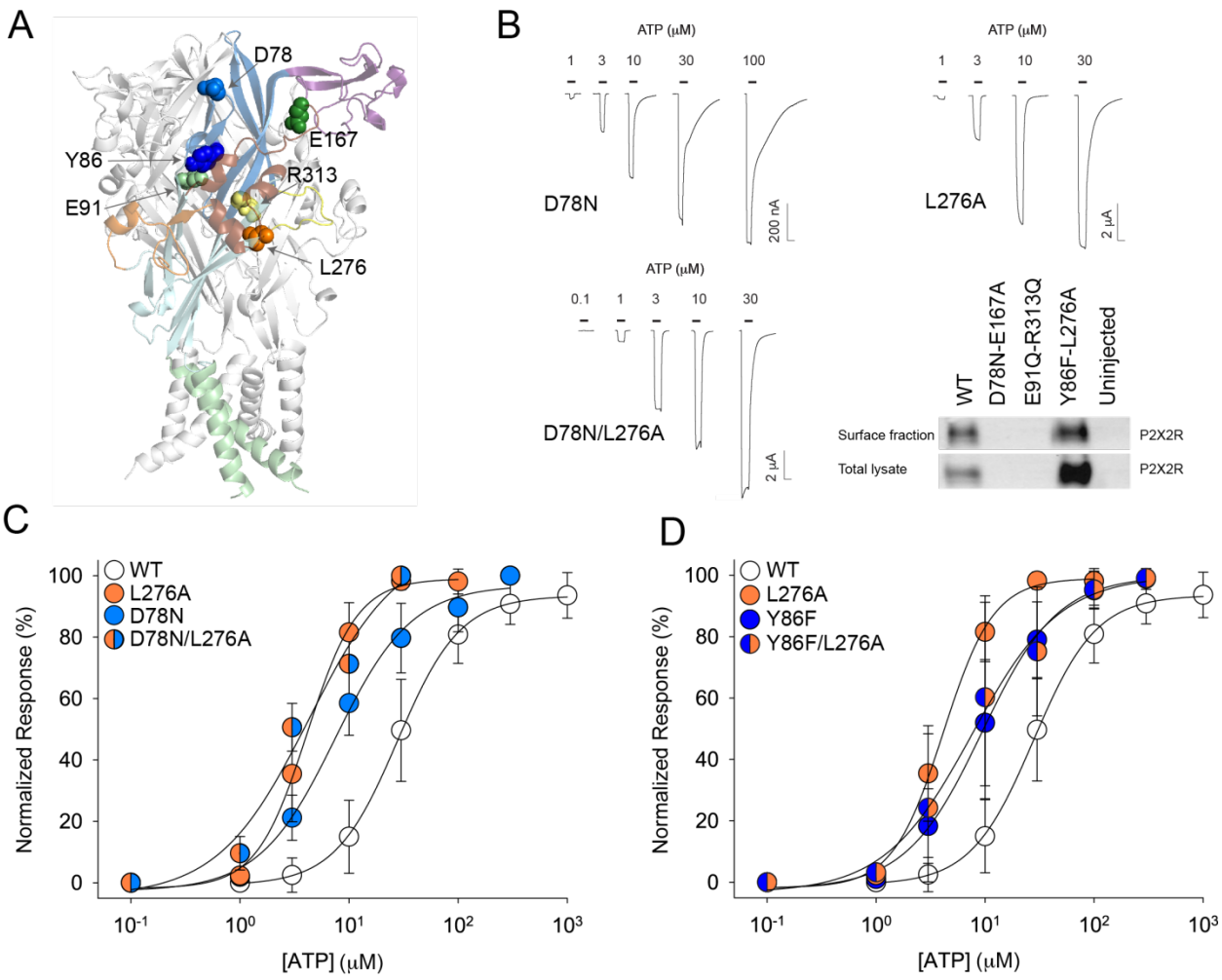

Figure 4: Characterization of double mutants disrupting different subunit interface. *(A) Homology model of rP2X2R with residues corresponding to the positions mutated shown as spheres (same colour scheme as Figure 2). (B) Example recordings of D78N, L276A and D78N/L276A and Western blot of surface fraction or total lysate extracted from oocytes expressing the indicated constructs (or uninjected oocytes). The uncropped blot is shown in Supplementary Figure 1. (C) and (D) Normalized ATP-elicited concentration-response data for WT (empty symbols), indicated single (single-colour symbols) and double mutants (split-colour symbols) P2X2Rs in response to increasing concentrations of ATP. Data are shown as mean ± S.D. (n = 4-24).*

Energetic coupling with residues not lining the subunit interface

Finally, we sought to assess if energetic coupling can also be observed for double mutants in which one of the mutations was located *away* from the subunit interface. We thus chose to generate the S122C and T123C single mutants in the head domain, which resulted in a pronounced left-shift in the ATP CRC (Table 1). Similarly, both the S122C/L276A and the T123C/L276A double mutants displayed a left-shifted EC_{50}

compared to that of the WT and exhibited strong energetic coupling (8.3 kJ mol^{-1} and 9.8 kJ mol^{-1}, respectively; Table 2). This was mirrored by the results obtained for the Y86F/T123C double mutant, which also showed high ATP apparent affinity (, Table 2) and strong energetic coupling (6 kJ mol^{-1}, Table 2). These findings suggest that pronounced energetic coupling is not unique to residues located at the subunit interface, but may be a more general property of the rP2X2R ECD.

DISCUSSION

Mutations of conserved side chains within a protein of interest typically disrupt function. In the context of LGICs, this means that mutations in the ECD, including those at or near the subunit interface, tend to result in increased EC_{50} values for ligands binding at the orthosteric binding site or more generally disrupt channel function. This has been observed for a variety of LGICs, such as GlyR α1, nAChR α7 and iGluRs (Braun et al., 2016; Iacobucci et al., 2021; Tang et al., 2018; Tang & Lummis, 2018; Weston et al., 2006). In fact, even mutational scans in the ECD of a close cousin of the P2X2R, the P2X1R, have established that the vast majority of mutations result in increased EC_{50} values (Ennion et al., 2000; Roberts & Evans, 2004, 2006). Similarly, mutations in or near the ATP-binding pocket of a variety of P2XR subtypes have been shown to greatly increase EC_{50} values (Bodnar et al., 2011; Gasparri et al., 2019; Hausmann et al., 2013; L. H. Jiang et al., 2000; Roberts et al., 2008; Zemkova et al., 2007). Here, however, we find that nearly 90% (20/23) of mutations designed to disrupt putative interactions across rP2X2R inter-subunit interfaces resulted in *lower* EC_{50} values. Importantly, this trend was independent of the chemical properties of the side chain in question, e.g. this was true for aromatic, hydrophobic and charged side chains (Table 1). This finding is consistent with previous P2X2R studies, which demonstrated that individual mutations of side chains lining the subunit interface in the ECD or TMD result in lower EC_{50} values or even constitutive activity (George et al., 2019; R. Jiang et al., 2010).

Given that many of the side chains mutated here are conserved across different P2XR isoforms (Kawate et al., 2009), it remains to be elucidated to what extent our findings apply to the other members of this receptor family. Also, in light of the lower EC_{50}s observed for mutations away from the subunit interface (S122C and T123C in this study, E167R and H319A/K in work by others (Clyne et al., 2002; Hausmann et al., 2013; Sattler et al., 2020)), we cannot exclude the possibility that the trend observed for mutations at the subunit interface is not a more general feature of the rP2X2R ECD (outside the ligand-binding pocket).

Finally, we sought to assess if combining two of the tested single mutants would indicate energetic coupling. To this end, we turned to double-mutant cycle analysis. Two of the mutant pairs (E91Q/R313Q and D78N/E167A) failed to express, but the remaining 10 pairs could be tested functionally (Table 2). Both

double mutants involving S190A (S190A/D78N and S190A/V80A) showed no signs of strong coupling (ΔΔG values of 1.3 and 0.7 kJ/mol, respectively), possibly due to the large physical distance between the two mutations/residues. By contrast, we observed strong energetic coupling for the remaining double mutants we tested, especially for side chains in relative close proximity within the structure (ΔΔG values >2.5 kJ/mol, see Table 2). Here, the E84Q/E91Q double mutant stood out in particular, with a ΔΔG value of 14.7 kJ/mol. This value is much higher than those observed in previous P2X2R studies (Hausmann et al., 2013; R. Jiang et al., 2010), but similar to that reported with side chains lining the ligand-binding site of a glutamate-gated chloride channel (Lynagh et al., 2017). Interestingly, strong energetic coupling was not restricted to double mutants along the subunit interface. In fact, the L276A-containing double mutants L276A/S122C and L276A/T123C both showed high ΔΔG values, although neither S122 and T123 are located at the subunit interface. This could suggest that residue pairs involving at least one interface side chain tend to be strongly coupled. However, it is also plausible that the strong coupling effects observed for S122 and T123 mutants are due to more global disruptions due to altered disulphide bond patterns in the cysteine-rich head domain (Lörinczi et al., 2012).

In conclusion, we find that mutations at the subunit interface of the rP2X2R ECD generally result in lower EC_{50} values, thus apparently favoring channel opening. We further demonstrate that double mutations involving these sites typically show strong energetic coupling, especially for sites within close proximity, revealing a tight interplay between residues in the ECD that likely stabilize a closed channel conformation. Although possibly not exclusive to inter-subunit locations or even ECD sites, these findings indicate that rP2X2Rs, unlike numerous other LGICs, have apparently not evolved for maximum agonist sensitivity. In support of this notion, their activation is fine-tuned by Mg^{2+}, which when bound to ATP renders it a very ineffective agonist (Li et al., 2013). It is thus tempting to speculate that P2X2Rs have evolved towards low levels of activity, possibly as a cellular protection mechanism against overstimulation or as a means to enable additional modulation of agonist sensitivity.

ACKNOWLEDGMENTS

We acknowledge the Lundbeck Foundation (R139-2012-12390; SAP), Carlsberg Foundation (2013-01-0439; SAP), Beckett Foundation (39414/42389; SAP), Hartmann Foundation (R73-A27283; SAP), Hørslev Foundation (203866; SAP). The authors thank Dr Thomas Grutter and members of the Pless labororatory for comments on the manuscript.

CONFLICT OF INTEREST STATEMENT

The authors declare no conflict of interest.

AUTHOR CONTRIBUTIONS

F.G., S.B. and M.H.P. conducted all experiments. F.G., M.H.P. and S.A.P. designed experiments and analysed data. F.G. and S.A.P wrote the manuscript with input from all authors. All authors have given approval to the final version of the manuscript.

METHODS

Chemicals

Adenosine 5′-triphosphate, disodium salt, hydrate (ATP, purity 99%) and salts were from Sigma-Aldrich.

Mutagenesis and expression of P2X2R in *Xenopus laevis* oocytes

Point mutations were introduced in the cDNA of the rat P2X2 receptor (rP2X2R, sub-cloned into the pNKS2 vector) via PCR with custom-designed primers (Eurofins Genomics) and PfuUltra II Fusion HS DNA polymerase (Agilent Technologies). Generally, positively charged amino acids (R and K) were substituted with Q; acidic residues (E and D) were mutated to Q and N, respectively; A was introduced instead of V, L or I; S was replaced by A and Y by F (to remove hydroxyl group) and H was mutated to L. The Ambion mMessage mMACHINE SP6 transcription kit (Thermo Fisher Scientific) was used to transcribe the rP2X2 cDNA to mRNA after linearization with Xho I (New England Biolabs). The reaction was purified with RNeasy columns (Qiagen) and mRNA was stored at – 80°C until use. Stage V-VI oocytes were surgically removed from *Xenopus laevis* frogs (anesthetized in 0.3% tricaine, according to license 2014-15-0201-00031, approved by the Danish Veterinary and Food Administration) and digested with collagenase (1.5 mg ml^{-1}, Roche), dissolved in OR2 (82 mM NaCl, 2.5 mM KCl, 1 mM $MgCl_2$, 5 mM HEPES adjusted to pH 7.4 with NaOH), under continuous shaking. Oocytes were incubated in OR2 at 18 °C and gently shaken until injection with mRNA. For electrophysiological recordings, WT and mutant rP2X2R mRNAs (concentration 50 - 3000 ng μl^{-1}) were injected into the oocyte cytoplasm with a Nanoliter 2010 injector (World Precision Instruments). The volume of mRNA injected varied depending on the construct (10-50 nl). Injected oocytes were incubated in OR3 solution (Leibovitz's L-15 medium (Life Technologies) with 5 mM L-glutamine, 2.5 mg ml^{-1} gentamycin, 15 mM HEPES, pH 7.6 with NaOH) and gently shaken at 18 °C until the day of the experiment.

Electrophysiological recordings and data analysis

One to two days after mRNA injection, oocytes were transferred into a recording chamber (Dahan et al., 2004) and continuously perfused with ND96 solution (in mM: 96 NaCl, 2 KCl, 1.8 $BaCl_2$, 1 $MgCl_2$, 5 HEPES, pH 7.4) through an automated, gravity-driven perfusion system operated by a ValveBank™ module (AutoMate Scientific). ATP solutions were freshly made prior to recordings. Solutions were prepared from agonist stocks (10 or 100 mM, stored at - 20°C) or directly weighted out and dissolved in ND96 to the desired final concentration (pH adjusted to 7.4 with NaOH). Oocytes were clamped at -40 mV and 10 sec application of increasing concentration of ATP were used to activate rP2X2Rs. Between each application, oocytes were perfused for 1 min with ND96 to allow for full recovery from desensitization. Currents were recorded using borosilicate microelectrodes (Harvard Apparatus, resistance of 0.3-2 MΩ), backfilled with 3 M KCl, and an Oocyte Clamp C-725C amplifier (Warner instrument Corp.). Current was acquired at 500 Hz and digitized via an Axon™ Digidata® 1550 interface and the pClamp (10.5.1.0) software (Molecular Devices). The signal was further digitally filtered at 10 Hz with an eight-pole Bessel filter for analysis and display. ATP-elicited concentration-response curves (CRCs) were obtained by plotting the normalized peak current amplitude against the ATP concentration for each individual recording and subsequently fitted to the Hill equation in Prism v7 (GraphPad) to calculate EC_{50} values. These were averaged and reported as mean ± SD. Data analysis was performed using Prism v7, significant differences were determined by one-way ANOVA with Dunnett's comparison to a control value (i.e WT). For figure display, a single fit to the average normalized response (± SD) is shown using SigmaPlot (SigmaPlot 13.0, Systat Software).

Cell surface biotinylation and Western blots

Oocytes were injected with 9.2 nl of mRNA coding for rP2X2 WT (0.05 µg $µl^{-1}$), 46 nl rP2X2-D78N-E167A (0.9 µg $µl^{-1}$), 46 nl rP2X2-E91Q-R313Q (0.9 µg $µl^{-1}$) and 9.2 rP2X2-Y86F-L276A (0.05 µg $µl^{-1}$). Following incubation in OR3 solution for 36 hrs at 18°C, the oocytes were washed twice with PBS-CM (in

mM: 137 NaCl, 2.7 KCl, 10 Na_2HPO_4, 1.8 KH_2PO_4, 0.1 $CaCl_2$, 1 $MgCl_2$) and surface proteins from 50 oocytes per construct were labeled using EZ-Link™ Sulfo-NHS-SS-Biotin (Thermo Fischer Scientific), dissolved to a final concentration of 1.25 mg ml^{-1} in ice cold PBS-CM. Following agitation for 30 min, the reaction was quenched for 30 min using quenching buffer (PBS-CM supplemented with 200 mM glycine). Next, the oocytes were lysed using lysis buffer (150 mM NaCl, 100 mM Tris-HCl, 0.1% SDS and 1% Triton-X-100) with added Halt protease inhibitor cocktail (1:100) (Thermo Fisher Scientific). Biotin-labeled surface proteins were isolated and purified using Pierce™ Spin Columns - Snap Cap (Thermo Fischer Scientific) with 500 µl of Pierce™ NeutrAvidin™ Agarose added to each column (Thermo Fisher Scientific). Purified surface proteins or total cell lysates were separated on a NuPage 3-8 % Tris-acetate protein gel (Thermo Fisher Scientific) at 200 V for 40 min and transferred to a PVDF membrane. Membranes were incubated with rabbit polyclonal anti-P2X2 (#APR-003, Alomone labs; 1:2000) and mouse anti-Na^+/K^+-ATPase (05-369; EMD Merck Millipore) at 4 °C overnight. Next, the membranes were washed 5×2 min with TBST (20 mM Tris-HCl, 150 mM NaCl, 0.1% Tween 20, pH 7.5) and incubated with secondary antibodies (IRDye 800CW goat-anti-rabbit (925-32211; LI-COR Biosciences) and IRDye 680RD goat-anti-mouse (926-68070; LI-COR Biosciences) for 1 hrs at RT in the dark. Finally, the membranes were washed 5×2 min in TBST before being imaged using a PXi gel imaging station (Syngene).

Double-mutant cycle analysis

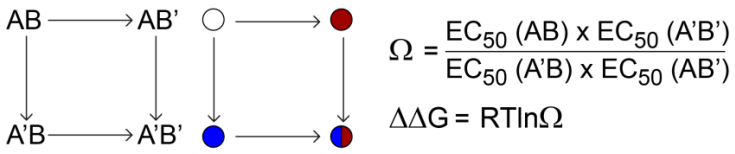

Double mutant cycle analysis. Principle of double mutant cycle analysis; AB represents WT protein, AB' and A'B- two different single mutants, A'B'- protein containing both mutations. Coupling coefficient Ω for the two residues- A and B- is calculated from the apparent EC_{50} values of WT, double mutant, and single mutants. Coupling energy (or free energy change) ΔΔG is further calculated from coupling coefficient Ω,

the gas constant R (8.314 J mol^{-1}. K^{-1}), room temperature T (298 K) (Horovitz, 1996; Schreiber & Fersht, 1995).

REFERENCES

Arulkumaran, N., Unwin, R. J., & Tam, F. W. K. (2011). A potential therapeutic role for P2X7 receptor (P2X7R) antagonists in the treatment of inflammatory diseases. *Expert Opinion on Investigational Drugs*, *20*(7), 897–915. https://doi.org/10.1517/13543784.2011.578068

Bodnar, M., Wang, H., Riedel, T., Hintze, S., Kato, E., Fallah, G., Gröger-Arndt, H., Giniatullin, R., Grohmann, M., Hausmann, R., Schmalzing, G., Illes, P., & Rubini, P. (2011). Amino acid residues constituting the agonist binding site of the human P2X3 receptor. *Journal of Biological Chemistry*, *286*(4), 2739–2749. https://doi.org/10.1074/jbc.M110.167437

Braun, N., Lynagh, T., Yu, R., Biggin, P. C., & Pless, S. A. (2016). Role of an Absolutely Conserved Tryptophan Pair in the Extracellular Domain of Cys-Loop Receptors. *ACS Chemical Neuroscience*, *7*(3), 339–348. https://doi.org/10.1021/acschemneuro.5b00298

Broom, D. C., Matson, D. J., Bradshaw, E., Buck, M. E., Meade, R., Coombs, S., Matchett, M., Ford, K. K., Yu, W., Yuan, J., Sun, S. H., Ochoa, R., Krause, J. E., Wustrow, D. J., & Cortright, D. N. (2008). Characterization of N-(adamantan-1-ylmethyl)-5-[(3R-amino-pyrrolidin-1-yl) methyl]-2-chloro-benzamide, a P2X7 antagonist in animal models of pain and inflammation. *Journal of Pharmacology and Experimental Therapeutics*, *327*(3), 620–633. https://doi.org/10.1124/jpet.108.141853

Burnstock, G. (1972). Purinergic Nerves. *Pharmacological Reviews*, *24*(3), 509–581.

Burnstock, Geoffrey. (2007). Physiology and pathophysiology of purinergic neurotransmission. In *Physiological Reviews* (Vol. 87, Issue 2, pp. 659–797). American Physiological Society. https://doi.org/10.1152/physrev.00043.2006

Carter, D. S., Alam, M., Cai, H., Dillon, M. P., Ford, A. P. D. W., Gever, J. R., Jahangir, A., Lin, C., Moore, A. G., Wagner, P. J., & Zhai, Y. (2009). Identification and SAR of novel diaminopyrimidines. Part 1: The discovery of RO-4, a dual P2X3/P2X2/3 antagonist for the treatment of pain. *Bioorganic and Medicinal Chemistry Letters*, *19*(6), 1628–1631. https://doi.org/10.1016/j.bmcl.2009.02.003

Chataigneau, T., Lemoine, D., & Grutter, T. (2013). Exploring the ATP-binding site of P2X receptors. In *Frontiers in Cellular Neuroscience* (Vol. 7, Issue Dec 30, p. 273).

https://doi.org/10.3389/fncel.2013.00273

Clyne, J. D., LaPointe, L. D., & Hume, R. I. (2002). The role of histidine residues in modulation of the rat P2X $_2$ purinoceptor by zinc and pH. *The Journal of Physiology*, *539*(2), 347–359. https://doi.org/10.1113/jphysiol.2001.013244

Coddou, C., Yan, Z., Obsil, T., Pablo Huidobro-Toro, J., & Stojilkovic, S. S. (2011). Activation and regulation of purinergic P2X receptor channels. *Pharmacological Reviews*, *63*(3), 641–683. https://doi.org/10.1124/pr.110.003129

Dahan, D. S., Dibas, M. I., Petersson, E. J., Auyeung, V. C., Chanda, B., Bezanilla, F., Dougherty, D. A., & Lester, H. A. (2004). A fluorophore attached to nicotinic acetylcholine receptor βM2 detects productive binding of agonist to the αδ site. *Proceedings of the National Academy of Sciences of the United States of America*, *101*(27), 10195–10200. https://doi.org/10.1073/pnas.0301885101

EMBL-EBI. (n.d.). *PDBePISA (Proteins, Interfaces, Structures and assemblies) at the European Bioinformatics Institute*. https://www.ebi.ac.uk/pdbe/prot_int/pistart.html

Ennion, S., Hagan, S., & Evans, R. J. (2000). The role of positively charged amino acids in ATP recognition by human P2X1 receptors. *Journal of Biological Chemistry*, *275*(38), 29361–29367. https://doi.org/10.1074/jbc.M003637200

Finger, T. E., Danilova, V., Barrows, J., Bartel, D. L., Vigers, A. J., Stone, L., Hellekant, G., & Kinnamon, S. C. (2005). Neuroscience: ATP signalling is crucial for communication from taste buds to gustatory nerves. *Science*, *310*(5753), 1495–1499. https://doi.org/10.1126/science.1118435

Gasparri, F., Wengel, J., Grutter, T., & Pless, S. A. (2019). Molecular determinants for agonist recognition and discrimination in P2X2 receptors. *Journal of General Physiology*, *151*(7). https://doi.org/10.1085/jgp.201912347

George, B., Swartz, K. J., & Li, M. (2019). Hearing loss mutations alter the functional properties of human P2X2 receptor channels through distinct mechanisms. *Proceedings of the National Academy of Sciences of the United States of America*, *116*(45), 22862–22871. https://doi.org/10.1073/pnas.1912156116

Hattori, M., & Gouaux, E. (2012). Molecular mechanism of ATP binding and ion channel activation in P2X receptors. *Nature*, *485*(7397), 207–212. https://doi.org/10.1038/nature11010

Hausmann, R., Günther, J., Kless, A., Kuhlmann, D., Kassack, M. U., Bahrenberg, G., Markwardt, F., & Schmalzing, G. (2013). Salt bridge switching from Arg290/Glu167 to Arg290/ATP promotes the closed-to-open transition of the P2X2 receptor. *Molecular Pharmacology*, *83*(1), 73–84. https://doi.org/10.1124/mol.112.081489

Hausmann, R., Kless, A., & Schmalzing, G. (2014). Key Sites for P2X Receptor Function and Multimerization: Overview of Mutagenesis Studies on a Structural Basis. *Current Medicinal Chemistry*, *22*(7), 799–818. https://doi.org/10.2174/0929867322666141128163215

Honore, P., Donnelly-Roberts, D., Namovic, M. T., Hsieh, G., Zhu, C. Z., Mikusa, J. P., Hernandez, G., Zhong, C., Gauvin, D. M., Chandran, P., Harris, R., Medrano, A. P., Carroll, W., Marsh, K., Sullivan, J. P., Faltynek, C. R., & Jarvis, M. F. (2006). A-740003 [N-(1-{[(cyanoimino)(5-quinolinylamino) methyl]amino}-2,2- dimethylpropyl)-2-(3,4-dimethoxyphenyl)acetamide], a novel and selective P2X7 receptor antagonist, dose-dependently reduces neuropathic pain in the rat. *Journal of Pharmacology and Experimental Therapeutics*, *319*(3), 1376–1385. https://doi.org/10.1124/jpet.106.111559

Horovitz, A. (1996). Double-mutant cycles: a powerful tool for analyzing protein structure and function. *Folding and Design*, *1*(6), R121–R126. https://doi.org/10.1016/S1359-0278(96)00056-9

Huang, L.-D., Fan, Y.-Z., Tian, Y., Yang, Y., Liu, Y., Wang, J., Zhao, W.-S., Zhou, W.-C., Cheng, X.-Y., Cao, P., Lu, X.-Y., & Yu, Y. (2014). Inherent Dynamics of Head Domain Correlates with ATP-Recognition of P2X4 Receptors: Insights Gained from Molecular Simulations. *PLoS ONE*, *9*(5), e97528. https://doi.org/10.1371/journal.pone.0097528

Iacobucci, G. J., Wen, H., Helou, M., Liu, B., Zheng, W., & Popescu, G. K. (2021). Cross-subunit interactions that stabilize open states mediate gating in NMDA receptors. *Proceedings of the National Academy of Sciences of the United States of America*, *118*(2). https://doi.org/10.1073/pnas.2007511118

Illes, P., Müller, C. E., Jacobson, K. A., Grutter, T., Nicke, A., Fountain, S. J., Kennedy, C., Schmalzing, G., Jarvis, M. F., Stojilkovic, S. S., King, B. F., & Di Virgilio, F. (2020). Update of P2X receptor properties and their pharmacology: IUPHAR Review 30. In *British Journal of Pharmacology* (Vol. 178, Issue 3). John Wiley and Sons Inc. https://doi.org/10.1111/bph.15299

Jarvis, M. F., Burgard, E. C., McGaraughty, S., Honore, P., Lynch, K., Brennan, T. J., Subieta, A., Van Biesen, T., Cartmell, J., Bianchi, B., Niforatos, W., Kage, K., Yu, H., Mikusa, J., Wismer, C. T., Zhu, C. Z., Chu, K., Lee, C. H., Stewart, A. O., … Faltynek, C. (2002). A-317491, a novel potent and selective non-nucleotide antagonist of P2X3 and P2X2/3 receptors, reduces chronic inflammatory and neuropathic pain in the rat. *Proceedings of the National Academy of Sciences of the United States of America*, *99*(26), 17179–17184. https://doi.org/10.1073/pnas.252537299

Jiang, L. H., Rassendren, F., Surprenant, A., & North, R. A. (2000). Identification of amino acid residues contributing to the ATP-binding site of a purinergic P2X receptor. *Journal of Biological Chemistry*, *275*(44), 34190–34196. https://doi.org/10.1074/jbc.M005481200

Jiang, R., Lemoine, D., Martz, A., Taly, A., Gonin, S., Prado De Carvalho, L., Specht, A., & Grutter, T. (2011). Agonist trapped in ATP-binding sites of the P2X2 receptor. *Proceedings of the National Academy of Sciences of the United States of America*, *108*(22), 9066–9071. https://doi.org/10.1073/pnas.1102170108

Jiang, R., Martz, A., Gonin, S., Taly, A., De Carvalho, L. P., & Grutter, T. (2010). A putative extracellular salt bridge at the subunit interface contributes to the ion channel function of the ATP-gated P2X2 receptor. *Journal of Biological Chemistry*, *285*(21), 15805–15815. https://doi.org/10.1074/jbc.M110.101980

Jiang, R., Taly, A., Lemoine, D., Martz, A., Cunrath, O., & Grutter, T. (2012). Tightening of the ATP-binding sites induces the opening of P2X receptor channels. *The EMBO Journal*, *31*(9), 2134–2143. https://doi.org/10.1038/emboj.2012.75

Karasawa, A., & Kawate, T. (2016). Structural basis for subtype-specific inhibition of the P2X7 receptor. *ELife*, *5*(Dec 9), e22153. https://doi.org/10.7554/eLife.22153

Kasuya, G., Fujiwara, Y., Takemoto, M., Dohmae, N., Nakada-Nakura, Y., Ishitani, R., Hattori, M., & Nureki, O. (2016). Structural Insights into Divalent Cation Modulations of ATP-Gated P2X Receptor Channels. *Cell Reports*, *14*(4), 932–944. https://doi.org/10.1016/j.celrep.2015.12.087

Kasuya, G., Fujiwara, Y., Tsukamoto, H., Morinaga, S., Ryu, S., Touhara, K., Ishitani, R., Furutani, Y., Hattori, M., & Nureki, O. (2017). Structural insights into the nucleotide base specificity of P2X receptors. *Scientific Reports*, *7*(1), 1–10. https://doi.org/10.1038/srep45208

Kasuya, G., Yamaura, T., Ma, X. B., Nakamura, R., Takemoto, M., Nagumo, H., Tanaka, E., Dohmae, N., Nakane, T., Yu, Y., Ishitani, R., Matsuzaki, O., Hattori, M., & Nureki, O. (2017). Structural insights into the competitive inhibition of the ATP-gated P2X receptor channel. *Nature Communications*, *8*(1). https://doi.org/10.1038/s41467-017-00887-9

Kawate, T., Michel, J. C., Birdsong, W. T., & Gouaux, E. (2009). Crystal structure of the ATP-gated P2X4 ion channel in the closed state. *Nature*, *460*(7255), 592–598. https://doi.org/10.1038/nature08198

Khakh, B. S., & North, R. A. (2012). Neuromodulation by Extracellular ATP and P2X Receptors in the CNS. In *Neuron* (Vol. 76, Issue 1, pp. 51–69). Elsevier. https://doi.org/10.1016/j.neuron.2012.09.024

Li, M., Silberberg, S. D., & Swartz, K. J. (2013). Subtype-specific control of P2X receptor channel signaling by ATP and Mg2+. *Proceedings of the National Academy of Sciences of the United States of America*, *110*(36), E3455–E3463. https://doi.org/10.1073/pnas.1308088110

Lörinczi, E., Bhargava, Y., Marino, S. F., Taly, A., Kaczmarek-Hájek, K., Barrantes-Freer, A., Dutertre, S., Grutter, T., Rettinger, J., & Nicke, A. (2012). Involvement of the cysteine-rich head domain in activation and desensitization of the P2X1 receptor. *Proceedings of the National Academy of Sciences of the United States of America*, *109*(28), 11396–11401. https://doi.org/10.1073/pnas.1118759109

Lynagh, T., Komnatnyy, V. V., & Pless, S. A. (2017). Unique contributions of an arginine side chain to ligand recognition in a glutamate-gated chloride channel. *Journal of Biological Chemistry*, *292*(9), 3940–3946. https://doi.org/10.1074/jbc.M116.772939

Mansoor, S. E., Lü, W., Oosterheert, W., Shekhar, M., Tajkhorshid, E., & Gouaux, E. (2016). X-ray structures define human P2X 3 receptor gating cycle and antagonist action. *Nature*, *538*(7623), 66–

71. https://doi.org/10.1038/nature19367

McCarthy, A. E., Yoshioka, C., & Mansoor, S. E. (2019). Full-Length P2X7 Structures Reveal How Palmitoylation Prevents Channel Desensitization. *Cell*, *179*(3), 659-670.e13. https://doi.org/10.1016/j.cell.2019.09.017

Roberts, J. A., Allsopp, R. C., El Ajouza, S., Vial, C., Schmid, R., Young, M. T., & Evans, R. J. (2012). Agonist binding evokes extensive conformational changes in the extracellular domain of the ATP-gated human P2X1 receptor ion channel. *Proceedings of the National Academy of Sciences of the United States of America*, *109*(12), 4663–4667. https://doi.org/10.1073/pnas.1201872109

Roberts, J. A., Digby, H. R., Kara, M., El Ajouz, S., Sutcliffe, M. J., & Evans, R. J. (2008). Cysteine substitution mutagenesis and the effects of methanethiosulfonate reagents at P2X2 and P2X4 receptors support a core common mode of ATP action at P2X receptors. *Journal of Biological Chemistry*, *283*(29), 20126–20136. https://doi.org/10.1074/jbc.M800294200

Roberts, J. A., & Evans, R. J. (2004). ATP binding at human P2X1 receptors: Contribution of aromatic and basic amino acids revealed using mutagenesis and partial agonists. *Journal of Biological Chemistry*, *279*(10), 9043–9055. https://doi.org/10.1074/jbc.M308964200

Roberts, J. A., & Evans, R. J. (2006). Contribution of conserved polar glutamine, asparagine and threonine residues and glycosylation to agonist action at human P2X1 receptors for ATP. *Journal of Neurochemistry*, *96*(3), 843–852. https://doi.org/10.1111/j.1471-4159.2005.03593.x

Sattler, C., Eick, T., Hummert, S., Schulz, E., Schmauder, R., Schweinitz, A., Unzeitig, C., Schwede, F., & Benndorf, K. (2020). Unravelling the intricate cooperativity of subunit gating in P2X2 ion channels. *Scientific Reports*, *10*(1), 1–13. https://doi.org/10.1038/s41598-020-78672-w

Schreiber, G., & Fersht, A. R. (1995). Energetics of protein-protein interactions: Analysis ofthe Barnase-Barstar interface by single mutations and double mutant cycles. *Journal of Molecular Biology*, *248*(2), 478–486. https://doi.org/10.1016/S0022-2836(95)80064-6

Stelmashenko, O., Compan, V., Browne, L. E., & North, R. A. (2014). Ectodomain movements of an ATP-gated ion channel (P2X2 receptor) probed by disulfide locking. *Journal of Biological Chemistry*,

289(14), 9909–9917. https://doi.org/10.1074/jbc.M113.542811

Stephan, G., Huang, L., Tang, Y., Vilotti, S., Fabbretti, E., Yu, Y., Nörenberg, W., Franke, H., Göröncsér, F., Sperlágh, B., Dopychai, A., Hausmann, R., Schmalzing, G., Rubini, P., & Illes, P. (2018). The ASIC3/P2X3 cognate receptor is a pain-relevant and ligand-gated cationic channel. *Nature Communications*, *9*(1). https://doi.org/10.1038/s41467-018-03728-5

Tang, B., Devenish, S. O., & Lummis, S. C. R. (2018). Identification of Novel Functionally Important Aromatic Residue Interactions in the Extracellular Domain of the Glycine Receptor. *Biochemistry*, *57*(27), 4029–4035. https://doi.org/10.1021/acs.biochem.8b00425

Tang, B., & Lummis, S. C. R. (2018). Multiple regions in the extracellular domain of the glycine receptor determine receptor activity. *Journal of Biological Chemistry*, *293*(36), 13889–13896. https://doi.org/10.1074/jbc.RA118.003088

Wang, J., Wang, Y., Cui, W. W., Huang, Y., Yang, Y., Liu, Y., Zhao, W. S., Cheng, X. Y., Sun, W. S., Cao, P., Zhu, M. X., Wang, R., Hattori, M., & Yu, Y. (2018). Druggable negative allosteric site of P2X3 receptors. *Proceedings of the National Academy of Sciences of the United States of America*, *115*(19), 4939–4944. https://doi.org/10.1073/pnas.1800907115

Weston, M. C., Gertler, C., Mayer, M. L., & Rosenmund, C. (2006). Interdomain interactions in AMPA and kainate receptors regulate affinity for glutamate. *Journal of Neuroscience*, *26*(29), 7650–7658. https://doi.org/10.1523/JNEUROSCI.1519-06.2006

Zemkova, H., Yan, Z., Liang, Z., Jelinkova, I., Tomic, M., & Stojilkovic, S. S. (2007). Role of aromatic and charged ectodomain residues in the P2X4 receptor functions. *Journal of Neurochemistry*, *102*(4), 1139–1150. https://doi.org/10.1111/j.1471-4159.2007.04616.x

Zhao, W. S., Wang, J., Ma, X. J., Yang, Y., Liu, Y., Huang, L. D., Fan, Y. Z., Cheng, X. Y., Chen, H. Z., Wang, R., & Yu, Y. (2014). Relative motions between left flipper and dorsal fin domains favour P2X4 receptor activation. *Nature Communications*, *5*. https://doi.org/10.1038/ncomms5189

Zhu, Y., Beudez, J., Yu, N., Grutter, T., & Zhao, H. B. (2017). P2x2 dominant deafness mutations have no negative effect on wild-type isoform: Implications for functional rescue and in deafness mechanism.

Frontiers in Molecular Neuroscience, *10*. https://doi.org/10.3389/fnmol.2017.00371

TABLES

Table 1: ATP-elicited concentration-response data (EC_{50}) shown as mean ± S.D. as well as number of experiments (n) for WT and single mutants lining the P2X2R inter-subunit interface. Significant differences were determined by unpaired t test. **, $p < 0.05$; ***, $p < 0.001$; ****, $p < 0.0001$; [a], residues in the TM domain of P2X2R; [b], residues away from the interface (S122, T123) or previously characterized (E167 in (Hausmann et al., 2013)).

rP2X2 construct	EC_{50} ± SD (µM)	n
WT	35.1 ± 14	24
Y43A[a]	0.7 ± 0.3****	6
Y43F[a]	11 ± 2**	5
S65A	1.7 ± 0.2****	6
I73A	56 ± 12**	6
D78N	9.3 ± 3****	11
K79Q	36 ± 10	6
V80A	93 ± 12****	5
E84Q	4.1 ± 2****	9
Y86F	11 ± 5****	10
E91Q	17 ± 7***	12
S122C[b]	3.4 ± 1****	6
T123C[b]	1.9 ± 0.3****	6
E167Q[b]	6.1 ± 2****	8
S190A	3 ± 0.4****	7
D209N	8.2 ± 3***	6
H213L	13 ± 5***	6
L276A	4.5 ± 1****	12
S284A	9.1 ± 4****	10
K293Q	3.5 ± 0.9****	10
Y295F	4.1 ± 1****	6
R313Q	13.7 ± 3***	9

Table 2: ATP-elicited concentration-response data (EC_{50}) shown as mean ± S.D. as well as number of experiments (n) for WT and double mutants both at different and same subunit interface. Coupling energy values (kJ/mol) calculated as described in material and method section. Significant differences were determined by unpaired t test. **, $p < 0.05$; ***, $p < 0.001$; ****, $p < 0.0001$; [a], residues located *away* from the subunit interface.

rP2X2 construct	EC_{50} ± SD (μM)	n	Coupling energy, ΔΔG, kJ/mol
WT	35.1 ± 14	24	ND
Y86F L276A	12 ± 9.8***	8	5.1
D78N L276A	3.7 ± 0.8***	4	2.8
D78N E167Q	ND	ND	ND
E91Q R313Q	ND	ND	ND
L276A S284A	8.6 ± 1***	5	4.9
Y86F K293Q	10 ± 1***	5	5.3
E84Q E91Q	749 ± 145****	4	14.7
S190A D78N	1.3 ± 0.3****	9	1.3
S190A V80A	11 ± 3****	9	0.7
L276A T123C[a]	7 ± 3***	4	8.3
L276AA S122C[a]	23 ± 13	4	9.8
Y86F T123C[a]	6.8 ± 1***	4	6

SUPPLEMENTARY INFORMATION

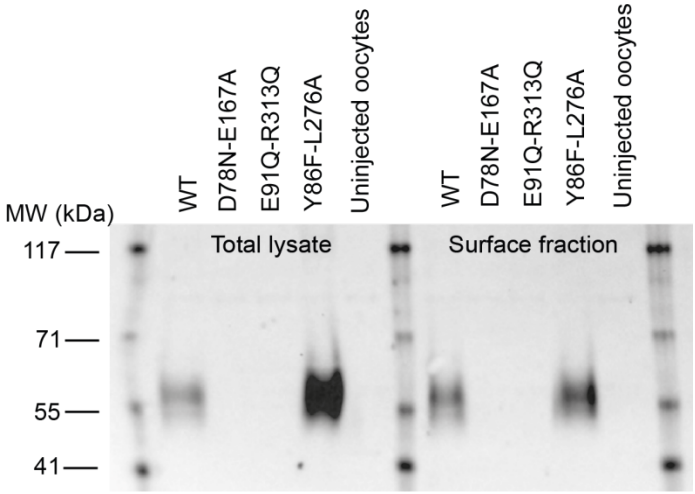

Supplementary Figure 1: *Uncropped Western blot for experiment shown in Figure 4. Surface fraction and total lysate extracted from oocytes expressing the indicated constructs (or uninjected oocytes) are shown.*

Supplementary Table 1: *List of residues lining the subunit interface of zfP2X4R that form H-bonds (HB) and/or electrostatic interactions (ION) in both conformational states (C, apo and O, ATP-bound) based on PISA analysis (default 4 Å cut-off for H-bonds and salt bridge). The atoms involved in the interactions are also shown in brackets (PDB nomenclature).* [a]*, residues known to form the ATP binding pocket therefore not analyzed further;* [b]*, interactions that were were different from or not found in an earlier study* (Hausmann et al., 2014)*. Note that residues involved in more than one interaction (i.e. S66) are listed only once in Table 1, and that due to sequence differences between P2X2 and P2X4 not all residues/interactions are conserved.*

Residue subunit A	Residue subunit B	Interaction type	State
S66 (OG)	R321 (NH2/1)	HB	O[b]
S66 (OG)	D323 (OD2)	HB	C
V67 (O)	R321 (NH2)	HB	O/C
T68 (OG1)	R321 (NH2)	HB	C[b]
K70 (NZ)	N296 (OD1)	HB	O[#]
I74 (O)	N140 (ND2)	HB	O
E84 (OE2)	K118 (NZ)	HB/ION	C[b]
R85 (NH2)	E310 (OE1)	HB/ION	O
I86 (N/O)	Q116 (OE1,NE2)	HB	O/C
I86 (O)	W167 (NE1)	HB	C [b]
D88 (OD1/2)	R312 (NH1/2)	HB/ION	O/C[a]
A90 (O)	Y302 (OH)	HB	O
D91 (OD1)	W167 (NE1)	HB	O
D91 (O/OD2)	Y302 (OH)	HB	O/C
D91 (OD2/1)	R312 (NH1)	HB/ION	O[a]
Y92 (OH)	E310 (OE1/2)	HB	C[b]
Q97 (NE2)	E98 (OE2)	HB	O[b]
D99 (OD2/1)	R321 (NH1/2)	ION	O
K193 (NZ)	A292 (O)	HB	O[b]
K193 (NZ)	G294 (O)	HB	O[b]
K193 (NZ)	V291 (O)	HB	C[b]
N195 (OD1)	N284 (N)	HB	O
N195 (OD1)	K285 (N)	HB	O
N195 (ND2)	L282 (O)	HB	C
R206 (NH1/2)	L282 (O)	HB	C
R206 (NH2)	N289 (OD1)	HB	O
R206 (NH2/1)	V291 (O)	HB	O
R206 (NH1)	A292 (O)	HB	O
S214 (OG)	D288 (OD1)	HB	C
S214 (OG)	N289 (N)	HB	C[b]
S214 (OG)	N290 (N/OD1)	HB	C
L217 (O)	R143 (NH2)	HB	O[b]
H219 (O)	R143 (NH1)	HB	O[b]
C220 (O)	R143 (NH1/2)	HB	O
K301 (NZ)	E310 (OE1/2)	HB/ION	O/C
Y303 (OH)	E310 (OE2)	HB	O/C
I335 (O)	Y45 (OH)	HB	C[b]